Vibrational Spectroscopy and Conformational Structure of Protonated Polyalanine Peptides Isolated in the Gas Phase

Timothy D. Vaden,*,† Tjalling S. J. A. de Boer,† John P. Simons,† Lavina C. Snoek,† Sándor Suhai,‡ and Béla Paizs*,‡

Physical and Theoretical Chemistry Laboratory, Chemistry Department, University of Oxford, South Parks Road, Oxford OX1 3QZ, United Kingdom, and German Cancer Research Center, Im Neuenheimer Feld 580, D-69120 Heidelberg, Germany

Received: January 4, 2008

The conformational structures of protonated polyalanine peptides, Ala_nH^+, have been investigated in the gas phase for $n = 3$, 4, 5, and 7 using a combination of resonant-infrared multiphoton dissociation (R-IRMPD) spectroscopy in the NH and OH stretch regions and quantum chemical calculations. Agreement between theoretical IR and experimental R-IRMPD spectral features has enabled the assignment of specific hydrogen-bonded conformational motifs in the short protonated peptides and revealed their conformational evolution under elevated-temperature conditions, as a function of increasing chain length. The shortest peptide, Ala_3H^+, adopts a mixture of extended and cyclic chain conformations, protonated, respectively, at a backbone carbonyl or the *N*-terminus. The longer peptides adopt folded, cyclic, and globular charge-solvated conformations protonated at the *N*-terminus, consistent with previous ion-mobility studies. The longest peptide, Ala_7H^+, adopts a globular conformation with the *N*-terminus completely charge-solvated, demonstrating the emergence of "physiologically relevant" intramolecular interactions in the peptide backbone. The computed conformational relative free energies highlight the importance of entropic contributions in these peptides.

1. Introduction

Understanding the folding mechanism of peptide chains into secondary structures requires some knowledge of the peptides' conformational landscapes. Identifying the inherent preferred conformations of isolated gas-phase peptides (i.e., in the absence of solvent) reveals a wealth of information regarding the local minima on their conformational landscapes. Detailed studies of neutral gas-phase peptides have been undertaken by numerous researchers, using ultraviolet (UV) and infrared (IR) spectroscopy combined with DFT and *ab initio* calculations. These have ranged from simple capped di- and tripeptides[1–4] to large systems such as Gramicidin.[5,6] In many cases, the results have highlighted important connections with "real-world" behavior by demonstrating the formation of traditional secondary-structure motifs like helices, β-sheets, and β- and γ-turns in the gas-phase species.[1,2,6,7] They have also demonstrated the sensitivity of peptide conformational landscapes to the presence of different intramolecular interactions.[2]

The structure and reactivity of gas-phase protonated peptides have been the subject of numerous studies, because the related chemistry is essentially the basis of protein identification in modern proteomics and systems biology.[8] Protonation of peptides, either at the *N*-terminus or at basic side chains (arginine, lysine, and histidine), introduces a positive charge to the system which can significantly alter the balance among competing intramolecular interactions. The conformational landscapes of protonated peptides are therefore often very different from those of their neutral counterparts. Protonated peptide structure has been investigated theoretically and mass spectrometrically using collision-induced dissociation (CID)[9] and gas-phase H/D exchange techniques,[10,11] and, more recently, ion-mobility experiments coupled with molecular dynamics simulations,[12–14] to infer the shapes of the protonated peptide ions. In this context, an important test case for comparing gas-phase to "real-world" protonated peptides is the polyalanine system. Long-chain polyalanine peptides form α-helices in solution at physiological pH.[15,16] While theoretical models predict that relatively short (∼5−10 residues) neutral polyalanine peptides form helices in the gas phase, protonated alanine-only helices are not predicted to be stable.[17] Jarrold and co-workers have combined ion-mobility experiments with molecular dynamics simulations to show that short protonated polyalanines, Ala_nH^+ ($n \leq 20$),[18] do not form helices, but instead form charge-solvated ("globular") conformations. Helical polyalanine peptide structures only form when the proton is relocated to the *C*-terminus by the addition of a lysine residue.[13,19]

Gas-phase ion-mobility/molecular dynamics studies give information about average shapes. Vibrational spectroscopy explores the specific conformations of short polypeptides, providing an important advantage. It helps to isolate and identify the different intramolecular interactions that control them and helps to understand their transition(s) from unfolded to folded peptides. This has inspired Polfer,[20] Grégoire,[21] and their co-workers to study protonated peptide structures (at room temperature) using resonant infrared multiphoton dissociation (R-IRMPD) spectroscopy in the amide I/II region, using a free-electron laser (FEL); Grégoire, Schermann, Desfrançois, Gaigeot, and their co-workers have also compared their experimental spectra to those computed through Car−Parrinello molecular dynamics (CPMD) simulations.[21,22] Most recently, Rizzo and co-workers have studied cold (∼10 K) protonated peptides, generated though electrospray ionization, using IR spectroscopy in the NH and OH stretch regions coupled with detection through UV-laser-induced

* timothy.vaden@chem.ox.ac.uk, B.Paizs@dkfz.de.
† University of Oxford.
‡ German Cancer Research Centre.

10.1021/jp800069n CCC: $40.75
Published on Web 04/30/2008

fragmentation (with the chromophore provided by the incorporation of an aromatic amino acid).[19,23,24]

We have recently developed an alternative scheme for generating protonated (ionic) molecules in a free jet expansion, via gas-phase photochemical protonation (enabling the study of a myriad of protonated molecules with or without aromatic chromophores), and characterizing their structures with R-IRMPD spectroscopy in the OH and NH stretch regions, supplemented by DFT calculations.[25–27] R-IRMPD spectra recorded in the OH/NH stretch region are particularly valuable since they provide direct information on H-bonded interactions and allow comparison to the structural information gained from measurements made in the amide I/II and "fingerprint" regions, accessed through FEL experiments. While the internal energy content of the protonated ions generated photochemically cannot be characterized precisely, both our experiments and order-of-magnitude calculations have suggested energy distributions corresponding to room temperature or slightly above,[25] comparable with those studied by Grégoire et al.[21] and comparable also with temperatures that are biologically relevant. This implies that their conformational energy landscapes will reflect entropic as well as energetic considerations. While this investigative technique at its present stage of development is not conformationally selective, it nevertheless can yield information about the distributions of conformer populations and characterize the evolution of peptide conformations as chains increase in length and complexity. Application of the photochemical protonation strategy to the alanine dipeptide in a "proof of concept" investigation[25] to provide its R-IRMPD spectra in the NH/OH stretch region identified the same "Trans-A1" unfolded structure that had been identified through the earlier FEL experiments.[22]

The current investigation builds upon this success, applying the photochemical protonation strategy more widely to explore the conformational landscapes of a series of protonated alanine polypeptides, Ala_nH^+, of steadily increasing chain length, $n = 3-7$, where folding into globular shapes can be anticipated.[18] Spectroscopic measurements conducted between 2500 and 4000 cm^{-1} coupled with modeling in conjunction with density functional theoretical and MP2 computations have been used to follow the formation and evolution of their charge-solvated shape and structure and in some cases allow the identification of specific conformations.

2. Experiment and Computational Methods

2.1. Experimental Methods. Protonated peptides were generated through the photochemical schemes 1−4, described in detail elsewhere,[25–27] in which intermolecular proton transfer follows resonance-enhanced 2-photon ionization (R2PI) of a phenol-peptide complex.

$$AH + B \rightarrow [AH - B] \quad (1)$$

$$[AH - B] + 2h\nu \rightarrow [AH^+ - B]\bullet \quad (2)$$

$$[AH^+ - B]\bullet \rightarrow A\bullet - BH^+ \quad (3)$$

$$A\bullet - BH^+ \rightarrow A\bullet + BH^+ \quad (4)$$

In the present context, AH represents phenol while B represents a peptide. Cold AH−B complexes were generated, step 1, by seeding gas-phase peptides into a pulsed supersonic expansion of phenol in argon carrier gas. The peptides were vaporized by ablating a peptide-coated graphite surface with the 1064 nm output of a Continuum Minilite Nd:YAG laser. Their complexes, [AH−B], passed through a skimmer into the extraction region of a linear time-of-flight (TOF) mass spectrometer (R. M. Jordan), where they were ionized, step 2, at ∼278 nm via R2PI using the frequency-doubled output of a Lamda-Physik FL2002 dye laser. Rapid, exothermic proton transfer within the ionized complexes, $[AH^+-B]\bullet$, from the phenol cation to the peptide, step 3, followed by endothermic loss of the phenoxy radical A•, step 4, generated the free protonated peptide ions, BH^+. Given the warm nature of the ions and the expected subnanosecond time scales of steps 1−4, the protonated peptides are likely to assume their free-energetically favored conformations irrespective of the initial [AH−B] conformations. Ala_3, Ala_4, and Ala_5 samples were obtained from Bachem (Germany), while Ala_7 samples were obtained from Celtek Peptides (USA).

The protonated ions were probed with R-IRMPD spectroscopy using the idler output (∼10−20 mJ/pulse, tunable from 2000−4000 cm^{-1}, with a bandwidth of ∼2 cm^{-1}) of a LaserVision KTP/KTA OPO/OPA laser system, tightly focused to a beam diameter of ∼800 μm, which intersected the ions 400 ns after the UV pulse, in a spatially distinct region downstream from the ionizing UV laser beam. Absorption of the IR photons led to dissociation through the R-IRMPD process.[28] The R-IRMPD spectra were recorded by monitoring the depletion of the (parent) protonated peptide ion as a function of the IR frequency, since the TOF mass spectra were too congested to unambiguously identify the fragment ions. Active baseline correction was employed to accommodate signal fluctuations: the experiment operated at 10 Hz, while the IR laser operated at 5 Hz.

The internal energy content of the protonated cations, although not well-characterized, is dictated primarily by the excess energy after two-photon ionization (at most ∼60 kJ mol^{-1}), the ΔH of the proton transfer reaction 3 (∼100 kJ mol^{-1}), and the binding energy of the $A\bullet-BH^+$ complex (estimated to be ∼75 kJ mol^{-1}).[25] The "temperatures" corresponding to internal energies of ∼85 kJ mol^{-1} would depend on the peptide size due to the vibrational heat capacities; for protonated Ala_4, with a heat capacity of ∼375 J mol^{-1} K^{-1}, the estimated "temperature" would be ∼250 K (∼150 K for Ala_7). However, it is also likely that the ions absorb an additional UV photon during ionization, thereby increasing the excess ion energy, and leading to "temperatures" in excess of 400 K. Furthermore, it is possible that water molecules (ever-present in the expansion) initially bound to the [AH−B] complex evaporate after ionization, thereby lowering the final internal energies. Assuming a water binding energy of 40 kJ mol^{-1} (consistent with literature values[29]), evaporation could lead to energies anywhere from 45 kJ mol^{-1} (if no additional UV photons are absorbed) to ∼100 kJ mol^{-1} or more (for additional UV absorption). The lack of any signal for hydrated ions in the TOF mass spectrum suggests the latter case is more likely, with "temperatures" of ∼300 K for protonated Ala_4, assuming internal energy of 100 kJ mol^{-1}. Given the spread of uncertainties, the analyses in this work assume temperatures of ∼350 K as a rough guide.

2.2. Calculations. All calculations were performed at the German Cancer Research Center in Heidelberg, Germany. A recently developed conformational search engine[8,20,30] devised to deal with protonated peptides was used to scan the potential energy surfaces (PES) of protonated Ala_n, $n = 3-5$ and 7. These calculations started with molecular dynamics simulations on the above ions including the *N*-terminal amino and for Ala_3 and Ala_4, the amide oxygen protonation forms using the Insight II program (Biosym Technologies, San Diego, CA) in conjunction with the AMBER force field,[31] modified in-house in order to enable the study of oxygen-protonated amide bonds.

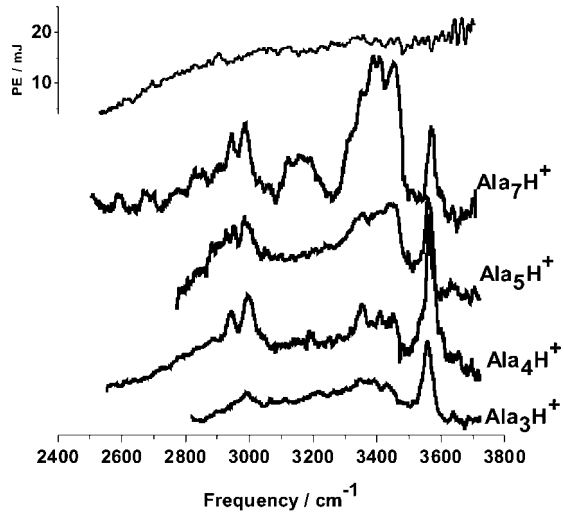

Figure 1. Summary of R-IRMPD spectra for Ala_nH^+, $n = 3$, 4, 5, and 7. All spectra were measured by monitoring the depletion of the parent molecular ion as a function of IR wavenumber. The IR laser power (PE, pulse energy, in mJ) throughout the spectral region is included (top trace) to demonstrate the likely attenuation of the true intensity of the bands at low wavenumbers. The sharp spikes in the power curve above 3500 cm^{-1} correspond to atmospheric H_2O absorption.

During the dynamics calculations, we used simulated annealing techniques to produce candidate structures for further refinement, applying full geometry optimization using the AMBER force field. These optimized structures were analyzed by a conformer family search program developed by us. This program groups optimized structures into families for which the most important characteristic torsion angles of the molecule are similar. The most stable species in the families were then fully optimized at the PM3, HF/3-21G, B3LYP/6-31G(d), and finally at the B3LYP/6-31+G(d,p) levels, and the conformer families were regenerated at each level. Finally, to have the most accurate possible description of the relative 0 K energies (the DFT energies are only of moderate accuracy), single point MP2/6-31+G(d,p) calculations were carried out for the energetically most favored structures for each Ala_nH^+ peptide. The total energies of the lowest-energy structures are presented in Table S1 (Supporting Information). Note that for all *ab initio* and DFT calculations the Gaussian set of programs[32] was used.

For the energetically most preferred structures, we have performed frequency calculations at the B3LYP/6-31G(d) level of theory. The relative energies were calculated by correcting the B3LYP/6-31+G(d,p) or MP2/6-31+G(d,p) total energies for zero-point vibrational energy (ZPE) and/or thermal and entropy contributions determined from the unscaled B3LYP/6-31G(d) frequencies. To reflect the experimental internal energy distributions (see above), relative free energies were computed at 350 K (as an illustrative guide) for each of the predicted conformers; the same free energy correction was applied to both DFT and MP2 energies. As the dominant contributions to the entropy are made by the low-frequency modes, which are poorly treated by harmonic-frequency approximations, the computed free energies are unlikely to be quantitatively accurate, but their relative values do provide a rough guide to the conformational flexibility of these systems at elevated internal energies.

3. Results

3.1. Overview. The R-IRMPD spectra of Ala_nH^+, $n = 3$, 4, 5, and 7, are summarized in Figure 1. The band at ~3550 cm^{-1} observed in all four spectra likely corresponds to the free carboxylic acid OH stretch, based on comparison with IR spectra recorded for both neutral[3] and protonated[24] amino acids. Its relative intensity and position suggests no involvement of the OH group in hydrogen bonding in any of the dominant conformer(s), though shoulders on this band for some species (for example, $Ala_4H^+$and Ala_7H^+) may hint at the presence of some weak hydrogen-bonded interactions. In general, though, the OH band is relatively sharp with a fwhm of ~25 cm^{-1} for all four species, significantly narrower than the fwhm of ~40 cm^{-1} observed for Ala_2H^+.[25] The bands below 3500 cm^{-1} appear to narrow somewhat from Ala_3H^+ to Ala_7H^+. The spectral broadening in Figure 1 most likely reflects overlapping sequence bands and the distribution of conformational populations, which are related to ion internal energy distributions. Thus, the polypeptide ions in the present study, where $n > 2$, appear to be cooler than the dipeptide studied previously and also appear to cool with increasing chain length, which is reasonable, since the larger peptides have more vibrational modes and thus higher heat capacities.

The remaining spectral features in Figure 1 can in principle correspond to NH stretch modes, CH stretch modes, and various overtone and combination bands. An important note here is that R-IRMPD detection is a complex process and its mechanism is not well-characterized;[28] it may even follow a different mechanism in the 2500−4000 cm^{-1} region than in the 1000−2000 cm^{-1} FEL region. Nevertheless, it is clear that a rough correlation exists between the intensities of bands associated with given vibrational modes detected through R-IRMPD and their corresponding "conventional" IR intensities, and the observation of overtone/combination bands is unlikely in view of their low expected IR intensities. Similarly, CH stretch modes, while certainly present, are unlikely to provide a major contribution to the intense bands observed below 3100 cm^{-1}, especially for Ala_4H^+, Ala_5H^+, and Ala_7H^+. Thus, the bands located between 2800 and 3500 cm^{-1} correspond predominantly to NH stretch modes.

The NH bands in Ala_3H^+ are broad and poorly resolved, but in general, they become narrower and more intense when the chain length is increased from Ala_4H^+ to Ala_7H^+. They fall into three broad zones, lying below 3100 cm^{-1}, between 3100 cm^{-1} and 3300 cm^{-1}, and between 3300 cm^{-1} and 3500 cm^{-1}. In the lowest wavenumber zone, the single, relatively weak, broad feature in Ala_3H^+ is replaced by an intense doublet in Ala_4H^+ through Ala_7H^+. An additional broad and poorly resolved feature centered around 3200 cm^{-1} appears in Ala_7H^+ and is absent in the other species, and the set of bands lying between 3300 and 3500 cm^{-1} becomes steadily more intense with increasing chain length.

Changes in the NH bands in the R-IRMPD spectra of the peptide series offer clues into the evolution of their three-dimensional conformational structures because of the sensitivity of the stretching modes to different hydrogen bonding configurations.[33,34] This evolution can be followed in Figure 1: as the chain length increases, a structural transition occurs at Ala_4H^+, signaled by the appearance of the intense doublet at low wavenumber. Another different "transition" can be identified in the Ala_7H^+ spectrum, signaled by the appearance of a new diffuse feature centered around 3175 cm^{-1} and the observation that the resolved IR bands tend to become significantly narrower as the chain length increases.

The diffuse character of the spectrum associated with Ala_3H^+ suggests a higher internal temperature in the shortest peptide and, perhaps also, the population of a broad distribution of

TABLE 1: ZPE-Corrected 0 K Relative Energies (ΔE) and Relative Free Energies (ΔG_{350}) for the Different Conformers of Each Ala_nH^+ peptide[a]

peptide	conformer label	ΔE[b]	ΔG_{350}[b]	ΔE[c]	ΔG_{350}[c]	ΔE[d]	ΔG_{350}[d]
Ala_3H^+	A_31	0.0	0.0	7.4	0.0	3.1	0.0
	A_32	1.4	2.7	9.8	3.8	5.7	3.8
	A_33	20.4	27.8	0.0	0.0	0.0	3.4
	A_34	21.2	25.9	4.4	1.7	4.6	5.9
Ala_4H^+	A_41	0.0	9.4	0.0	0.0		
	A_42	21.2	27.5	9.7	6.7		
	A_43	19.4	25.1	12.1	8.4		
	A_44	9.2	0.0	46.0	27.3		
Ala_5H^+	A_51	1.5	0.0	17.5	3.9		
	A_52	2.8	6.2	8.7	0.0		
	A_53	1.0	9.6	8.5	4.8		
	A_54	0.0	12.3	0.0	0.2		
Ala_7H^+	A_71	4.4	0.0	18.9	14.0		
	A_72	0.0	0.4	0.0	0.0		
	A_73	7.9	3.0	10.1	4.9		

[a] All values are in kJ mol^{-1}. [b] B3LYP/6−31+G(d,p)//B3LYP/6−31+G(d,p) energies, with unscaled B3LYP/6−31G(d) frequencies used for ZPE and free energetic contributions. [c] MP2/6−31+G(d,p)//B3LYP/6−31+G(d,p) energies, with unscaled B3LYP/6−31G(d) frequencies used for ZPE and free energetic contributions. [d] MP2/6−311+G(d,p)//B3LYP/6−311+G(d,p) energies, with unscaled B3LYP/6−311+G(d,p) frequencies used for ZPE and free energetic contributions.

conformers reflecting a dynamic and flexible character. The appearance of the strongly shifted doublet bands between 2900 cm^{-1} and 3000 cm^{-1} when $n \geq 4$ indicates a population of conformer(s) with strongly hydrogen-bonded NH groups. Similarly, the appearance of the moderately displaced bands between 3100 and 3300 cm^{-1} in the spectrum of Ala_7H^+ indicates the existence of conformational structure(s) with medium-strength hydrogen bonds.

This initial qualitative inspection of the R-IRMPD spectra of the Ala_nH^+ peptides already suggests a transition from loose and flexible structures to folded structures bound by tighter hydrogen bonds. More quantitative structural assignments can be achieved through comparisons with the vibrational spectra of the set of low-energy conformers predicted through DFT calculations; their relative energies (ΔE, kJ mol^{-1}) and free energies (ΔG_{350}, kJ mol^{-1}) calculated at an upper limit temperature of 350 K are listed in Table 1. The table includes the results of DFT calculations and also more accurate (single point) MP2 calculations based upon the DFT structures. Since the relative energetic ordering varies with the level of theory, their quantitative values have been treated with some caution, and comparisons with experiment are based primarily on the quality of the fit between the recorded vibrational spectra and the "library" of computed spectra.

3.2. Ala_3H^+. A recent investigation of Ala_3H^+ by Wu and McMahon[35] using a combination of R-IRMPD spectroscopy in the FEL region (1000−2000 cm^{-1}) and DFT and MP2 calculations supported the identification of Ala_3H^+ conformers protonated at a backbone carbonyl oxygen. Figure 2A presents the structures of its low-energy conformers, including both *O*-protonated (A_31 and A_32) and *N*-terminal-protonated (A_33 and A_34) peptides. A_32 and A_34 correspond to the published AAAH02 and AAAH01 structures,[35] respectively. A_31 was not identified in ref.[34] The published AAAH03 and AAAH04 structures[35] are energetically less favored than A_31 or A_33, respectively; therefore, we do not discuss them in detail.

The *O*-protonated conformers are very similar, differing only in their central ϕ and Ψ dihedral angles, and their computed

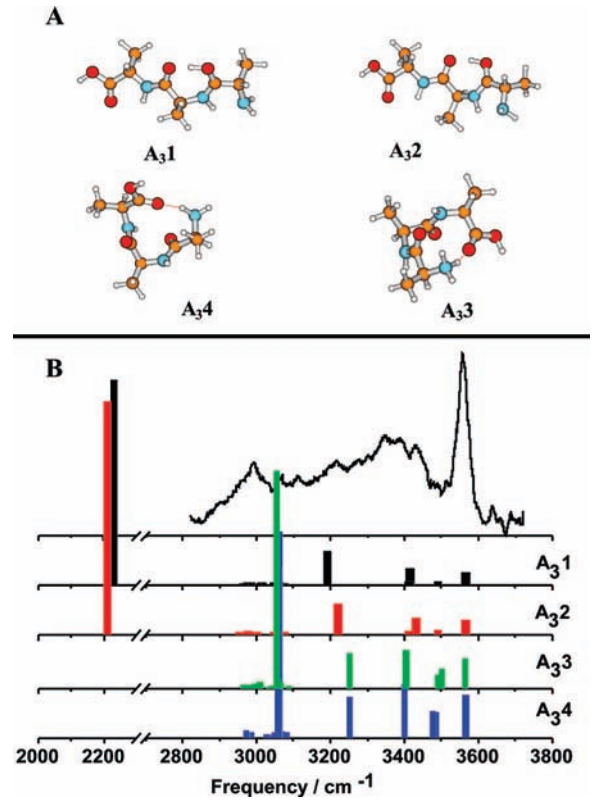

Figure 2. Summary of DFT calculations for Ala_3H^+. (A) Structures of four low-energy conformers (three structures very similar to A_31 and A_32 were also identified but are not shown here). (B) Theoretical frequencies, presented as wavenumbers (scaled by 0.97; see text for details), and relative IR intensities for the four conformers, shown as stick spectra for comparison with the experimental R-IRMPD spectrum (upper trace). The low-intensity CH modes are centered around 3000 cm^{-1} and will not be used for future assignments.

structures incorporate an $OH^+ \rightarrow O{=}C$ hydrogen bond (between the protonated backbone carbonyl and a neighboring carbonyl) and an $NH \rightarrow NH_2$ hydrogen bond (between a backbone NH and the *N*-terminus). Three other carbonyl-protonated conformers, ranging from ∼(5−15) kJ mol^{-1} higher in energy than A_31 (at both DFT and MP2 levels), were also identified, but these are not shown because their structures and their predicted spectra were virtually indistinguishable from those of A_31 and A_32. The other pair of low-energy conformers shown in Figure 2A, A_33 and A_34, are protonated at the *N*-terminus. Their computed structures, which differ only in the ϕ and Ψ angles of the central Ala residue, incorporate an $NH^+ \rightarrow O{=}C$ "charge-solvating" hydrogen bond between the *N*- and *C*-termini.

The DFT frequencies (presented as wavenumbers) and IR intensities associated with the conformational structures shown in Figure 2A are presented as stick spectra in Figure 2B. The theoretical frequencies are all scaled by 0.97 (the ratio of the experimental to the theoretical OH stretch frequency of protonated phenylalanine[24] computed at the B3LYP/6-31G* level). In all four conformations, this brings the mode at highest frequency, the free OH stretch, into close agreement with each of the experimental spectra. The theoretical spectra associated with the *O*-protonated (A_31 and A_32) and *N*-protonated (A_33 and A_34) conformers present two pairs of characteristic signatures, but *within* each pair they are very similar; the differences in ϕ and Ψ angles do not significantly affect the NH or OH stretches.

In A_31 and A_32, the asymmetric and symmetric free NH stretches of the *N*-terminus are associated with the bands at

~3496 and ~3416 cm^{-1} and the mode at ~3400 cm^{-1} corresponds to the free backbone NH. The mode at ~3200 cm^{-1} is associated with the hydrogen-bonded backbone NH, and the intense band predicted at ~2200 cm^{-1} is the hydrogen-bonded OH^+ stretch of the protonated backbone carbonyl group. The NH mode assignments for the *N*-terminal-protonated conformations, A_33 and A_34, are similar to those in the A_31 and A_32. The modes at ~3482 cm^{-1} correspond to free backbone NH stretches, while those at ~3225 and ~3400 cm^{-1} are the free *N*-terminal NH^+ stretches. The mode at ~3060 cm^{-1}, which is associated with the hydrogen-bonded *N*-terminal NH stretch, is strongly shifted from the free NH stretches around ~3400 cm^{-1} because of the cationic nature of the NH^+ bond (analogous to $OH^+ \rightarrow$ OH hydrogen bonds in protonated water clusters[36,37]). The CH stretch modes are predicted to lie at ~3000 cm^{-1} in all four conformers.

Within the measured wavenumber range (the cutoff below 2500 cm^{-1} is necessitated by the low IR laser power, ≤1 mJ/pulse which limits the range of R-IRMPD detection), the predicted spectra for A_31 and A_32 appear to agree with the experimental spectrum, although the relatively weak feature at ~3000 cm^{-1} is not supported by predicted NH stretch transitions. While in principle this band could be associated with the predicted CH modes, their excitation is unlikely to account completely for this feature, given its intensity (*vide supra*). The spectra predicted for the extended, carbonyl-protonated Ala_3H^+ conformers A_33 and A_34 do display an intense IR band at ~3000 cm^{-1}, although its relatively low (experimental) intensity (*c.f.* Ala_4H^+, *vide infra*) suggests that their population, and that of other conformers like them with similar energies, is low. Thus, both experiment and DFT calculations identify charge-solvated species like A_33 and A_34 as only minor contributors to the vibrational spectrum of the Ala_3H^+ peptide. The poor spectral resolution may well reflect contributions from additional (unfolded) conformers or, in the context of CPMD simulations of Ala_2H^+,[22] dynamic interconversion between them.

The MP2 relative energies (Table 1) show quite different trends. While the *O*-protonated species are very favorable at the DFT level, they are slightly *un*favorable at the MP2 level, at 0 K. However, at 350 K the lowest-energy *O*-protonated species (A_31) and lowest-energy *N*-protonated species (A_33) are isoenergetic. MP2/6-311+G(d,p)//B3LYP/6-311+G(d,p) energetics included in Table 1 support this trend: A_31 and A_33 "switch" energetically from 0 to 350 K, with A_33 being unfavorable by slightly more than k_BT. Furthermore, QCISD/6-31+G(d,p)//B3LYP/6-31+G(d,p) energetics for structures A_31 and A_33 show that at 0 K A_33 is favored by 4.8 kJ mol^{-1} while at 350 K A_31 is favored by 2.6 kJ mol^{-1}, supporting the MP2 results in Table 1. These results suggest a mixture of *N*- and *O*-protonated Ala_3H^+conformations, which very likely interconvert. This suggestion would (partially) explain the low resolution of our spectrum and agrees reasonably well with the experiment (as well as the work of Wu and McMahon[35]), as the R-IRMPD spectrum can be explained with predominantly *O*-protonated Ala_3H^+ with some contribution from *N*-protonated species. Therefore, our results are in good agreement with previous work, and they also highlight the importance of entropy in these peptide systems. It is worth noting here that the most favored *O*-protonated species have a nearly linear backbone stabilized by both hydrogen bonds and charge delocalization. Comparison of the theoretical data suggests that this charge-delocalization effect is overestimated by the applied DFT model.

3.3. Ala_4H^+. The structures predicted for Ala_4H^+ are shown in Figure 3A. A_41, A_42, and A_43 are protonated at the *N*-terminus. The lowest-energy conformer, A_41, presents a charge-solvating $NH^+ \rightarrow O{=}C$ hydrogen bond between the *N*- and *C*-termini, and a hydrogen bond between the *C*-terminal OH and a neighboring backbone carbonyl. In the two intermediate conformers, A_42 and A_43, the charge-solvating interaction is present but the carboxylic acid is free. In A_42, there is a single $NH^+ \rightarrow O{=}C$ hydrogen bond to a backbone carbonyl (not the *C*-terminus), whereas in A_43, two $NH^+ \rightarrow O{=}C$ hydrogen bonds—one in a charge-solvating interaction with the *C*-terminus and one with a neighboring carbonyl—are predicted. A_44 is protonated at a backbone carbonyl and adopts an extended structure analogous to the conformer A_31, shown in Figure 2A.

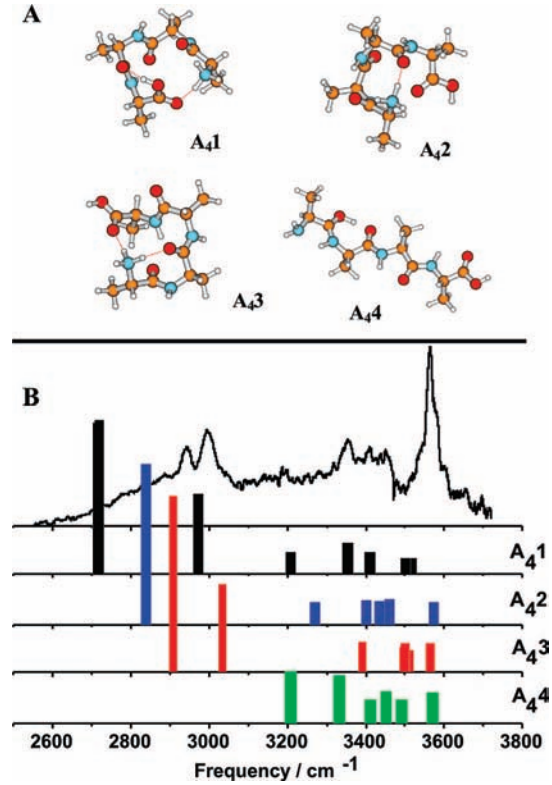

Figure 3. Summary of DFT calculations for Ala_4H^+. (A) Structures of four low-energy conformers. A_41 to A_43 are protonated at the *N*-terminus, while A_44 is protonated at a backbone carbonyl. (B) Theoretical frequencies, presented as wavenumbers, (scaled by 0.97) and relative IR intensities for the four conformers are shown as stick spectra in comparison to the experimental R-IRMPD spectrum (upper trace). CH modes are omitted.

The theoretical IR spectra for the Ala_4H^+ conformers are shown in Figure 3B. For A_41, free backbone NH stretches are associated with the modes at 3498 and 3515 cm^{-1} and the mode at ~3350 cm^{-1} corresponds to a backbone NH hydrogen-bonded to a neighboring carbonyl. Similarly, free *N*-terminal NH^+ stretches generate the vibrational modes at ~3200 and 3400 cm^{-1}, while the band at ~2700 cm^{-1} corresponds to the charge-solvating NH^+ ($NH^+ \rightarrow O{=}C$) vibration. The mode at ~2975 cm^{-1} is the hydrogen-bonded OH stretch. The theoretical spectrum for A_42 predicts a free *C*-terminal OH at 3572 cm^{-1} (absent in A_41) and free NH modes at 3435 and 3455 cm^{-1}. The free NH^+ stretch modes lie at 3272 and 3402 cm^{-1}, while the hydrogen-bonded NH^+ stretch is predicted at 2840 cm^{-1}. This vibration is higher in frequency than the corresponding vibration in A_41, likely because the *N*-terminus → backbone (A_42) is weaker than the *N*-terminus → *C*-terminus interaction (A_41). The highest-frequency mode in the conformation A_43, is the free OH stretch: the free backbone NH stretch lies at

~3500 cm^{-1}, the free *N*-terminal NH$^+$ stretch is at ~3390 cm^{-1}, and the two hydrogen-bonded NH$^+$ stretches are located at ~2900 cm^{-1} (corresponding to the charge-solvating *N*-terminus-*C*-terminus hydrogen bond) and at ~3040 cm^{-1} (corresponding to the remaining NH$^+$→ O═C interaction). The vibrational mode assignments for the spectrum associated with the extended, carbonyl-protonated conformer, $A_4$4, are similar to those of $A_3$1, shown in Figure 2; an intense hydrogen-bonded OH$^+$ stretch band (not shown) is predicted at ~2200 cm^{-1}. Note that the CH modes are omitted from Figure 3B (and subsequent analyses, *vide infra*); these modes are predicted to appear as a weak set of transitions around ~3000 cm^{-1}, identical to the theoretical Ala_3H^+ spectra in Figure 2B, more or less independent of differing conformational structures.

Comparing the experimental and theoretical spectra in Figure 3B, the appearance of the sharp band at ~3550 cm^{-1}, which most likely corresponds to a free OH (as opposed to a free NH) stretch based on its position, indicates a strong contribution from one or both of the conformers $A_4$2 and $A_4$3 ($A_4$4 is excluded based on its very high MP2 energy; see Table 1); $A_4$1 lacks a free OH mode and is therefore likely a minor conformer on the basis of free OH band intensity. The intense doublet bands observed at 2996 and 2943 cm^{-1} could be taken to favor $A_4$3, which presents two NH$^+$ → O═C vibrations in this region, but the bands could also reflect some contributions from the two (lower-energy) conformers $A_4$1 and $A_4$2. Note that the weak R-IRMPD feature at ~3200 cm^{-1}, which would support the identification of $A_4$2, is reproducible. The vibrational mode in $A_4$1, predicted at 2715 cm^{-1} (or, for that matter, the mode at ~2800 cm^{-1} in $A_4$2), could be difficult to detect in the R-IRMPD spectrum because of the diminishing OPO laser power in this region (*c.f.* the laser power curve shown in Figure 1, noting that the power at 2700 cm^{-1} is half that at 3000 cm^{-1}). While $A_4$1 is likely minor due to the absence of a free OH, given the results we cannot differentiate between $A_4$2 and $A_4$3, and both are likely to be present, although calculated to be somewhat higher in energy. (Given the energetic inaccuracies, these should not be taken too literally, though the ΔG_{350} values listed in Table 1 identify them as entropically favored.) Taken together, these results favor the population of cyclic, charge-solvated Ala_4H^+ conformations protonated at the *N*-terminus, $A_4$2 and A_4, unlike Ala_3H^+, where the contribution from such charge-solvated conformations is minimal.

3.4. Ala_5H^+. Our calculations predict four types of low-energy conformation in Ala_5H^+, each one charge-solvated and protonated at the *N*-terminus. Their structures, shown in Figure 4A, are closely analogous to the $A_4$2 and $A_4$3 conformers of Ala_4H^+. $A_5$1 presents a cyclic charge-solvated structure (with a single NH$^+$ →O═C hydrogen bond) analogous to $A_4$2; $A_5$2, with two *N*-terminal NH$^+$ → O═C hydrogen bonds, presents a globular structure, analogous to $A_4$3. $A_5$3 and $A_5$4 are similar to $A_5$2 except for the additional presence of hydrogen-bonded *C*-terminal OH groups: $A_5$3 presents an OH hydrogen bond to the Ala(2)-Ala(3) carbonyl, while $A_5$4 presents a similar interaction with its neighboring residue.

The theoretical spectra associated with each of the computed Ala_5H^+ conformers are shown in Figure 4B. In the same manner that conformational structures $A_5$1 and $A_5$2 are analogous to $A_4$2 and $A_4$3, respectively, their predicted IR spectra are also analogous. The calculations for the single hydrogen-bonded-NH$^+$ structure, $A_5$1, predict a free OH at 3566 cm^{-1}, free (and weakly hydrogen-bonded) NH backbone, and NH$^+$ modes from ~3300 to ~3500 cm^{-1}, and a hydrogen-bonded NH$^+$ mode at 2815 cm^{-1}. In the globular $A_5$2 conformation, they predict a

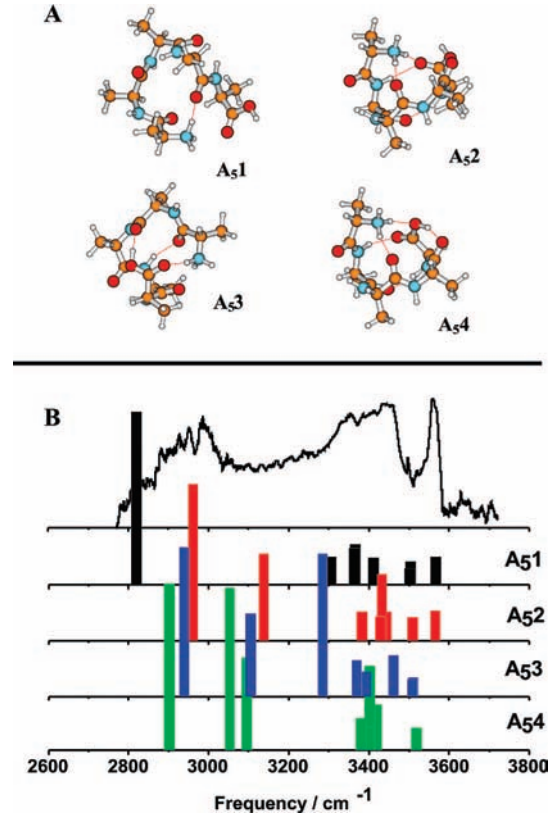

Figure 4. Summary of DFT calculations for Ala_5H^+. (A) Structures of four low-energy conformers. (B) Theoretical frequencies, presented as wavenumbers (scaled by 0.97), and relative IR intensities for the four conformers are shown as stick spectra in comparison to the experimental R-IRMPD spectrum (upper trace). CH modes are omitted.

free OH stretch at 3566 cm^{-1}, a cluster of free NH and NH$^+$ modes around ~3400 cm^{-1}, and two hydrogen-bonded NH$^+$ modes at 3140 cm^{-1} (NH$^+$ bonded to a backbone carbonyl) and 2965 cm^{-1} (NH$^+$ bonded to the *C*-terminus). The theoretical spectra for $A_5$3 and $A_5$4 are somewhat more complicated. In the $A_5$3 structure, there are two hydrogen-bonded NH$^+$ → O═C modes at 2940 and 3105 cm^{-1}, free NH and NH$^+$ modes between 3350 and 3500 cm^{-1}, and an intense hydrogen-bonded OH mode at 3285 cm^{-1}, while the spectrum predicted for $A_5$4 shows free NH$^+$and both free and weakly hydrogen-bonded NH modes around ~3400 cm^{-1}, two hydrogen-bonded NH$^+$ modes between 3000 and 3100 cm^{-1}, and a hydrogen-bonded OH stretch at ~2900 cm^{-1}.

Like Ala_3H^+ and Ala_4H^+, the band at ~3575 cm^{-1} in the experimental R-IRMPD spectrum (Figure 4B) most likely corresponds to a free OH stretch, indicating strong contributions from $A_5$1, $A_5$2, or both. Assessment of their relative contributions was clouded initially by the broad and poorly resolved absorption between 3000 and 3300 cm^{-1}, associated with free and, perhaps, weakly hydrogen bonded NH/NH$^+$ modes, but when the corresponding R-IRMPD spectrum was recorded at lower power, using pulse energies ~10 mJ rather than ~20 mJ, the resolution was much improved; see Figure 5. The IR bands in this region certainly appear more consistent with a major contribution from the globular structure, $A_5$2, rather than the cyclic $A_5$1 or for that matter, $A_5$3. Indeed, $A_5$2 is the most energetically favorable (Table 1). The two strongly hydrogen-bonded NH modes could correspond to the two IR peaks appearing at 2985 and 2940 cm^{-1} (despite the poor agreement with the band predicted at ~3100 cm^{-1}) or to an underlying

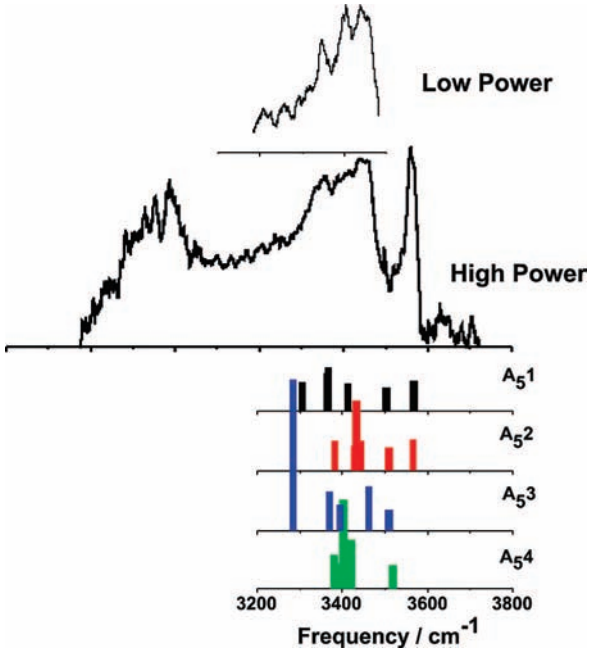

Figure 5. Comparison of Ala_5H^+ R-IRMPD spectrum measured at IR laser pulse energies of ~20 mJ (lower trace) and ~10 mJ (upper trace). The predicted IR transitions in this frequency region, included at the bottom of the figure, favor its assignment principally to the conformer A_52, with possibly a significant contribution from A_54.

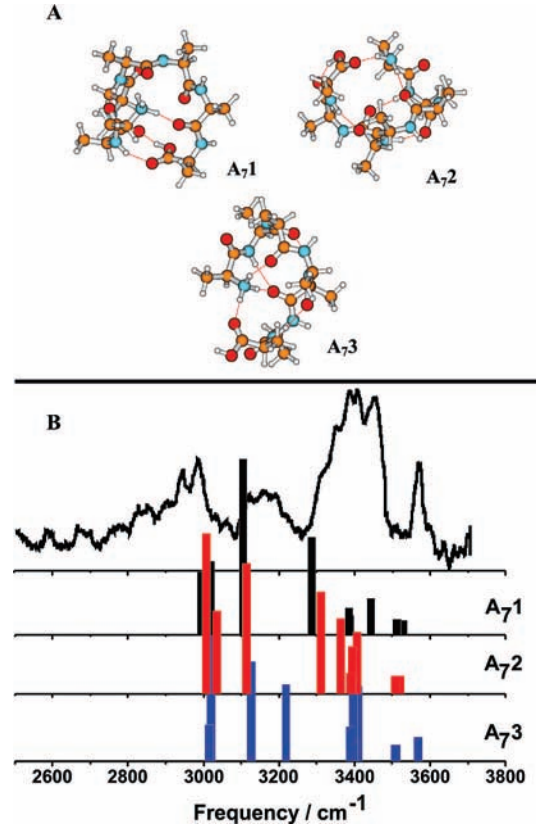

Figure 6. Summary of DFT calculations for Ala_7H^+. (A) Structures of four low-energy conformers. (B) Theoretical frequencies, presented as wavenumbers (scaled by 0.97), and relative IR intensities for the four conformers are shown as stick spectra in comparison to the experimental R-IRMPD spectrum (upper trace). CH modes are omitted.

contribution from the conformation A_54, calculated to be very favorable energetically. Therefore, while the Ala_5H^+ R-IRMPD spectrum could be explained by some combination of all four theoretical conformers, it does appear that A_52 is dominant (with possibly a significant contribution from A_54) based on the spectral comparisons in Figure 5 and the energetics of Table 1.

3.5. Ala_7H^+. The theoretical calculations predict three low-energy conformers of Ala_7H^+; all the alternative conformers are predicted to lie at significantly higher energies. Those at low energy are each protonated at the *N*-terminus and their structures are shown in Figure 6A. All three present several different types of NH → O=C hydrogen bond, and conformers A_71 and A_72 also incorporate a *C*-terminal hydrogen-bonded OH. Each of the structures contains charge-solvating NH^+ → O=C hydrogen bonds involving one (A_71), two (A_72), or all three NH^+ groups (A_73). The theoretical and experimental spectra are compared in Figure 6B. The predicted spectra are fairly complex, as expected for such a large system. The free NH and NH^+ modes in A_71 and A_72 lie between 3400 and 3525 cm^{-1}, their weakly hydrogen-bonded NH modes lie between 3300 and 3400 cm^{-1}, a hydrogen-bonded OH stretch is predicted around ~3100 cm^{-1}, and hydrogen-bonded NH^+ modes are predicted below 3000 cm^{-1}. In A_73, a free OH stretch mode is predicted at 3568 cm^{-1}, all of its free and weakly hydrogen-bonded NH/NH^+ modes are at ~3400 cm^{-1}, and the three hydrogen-bonded NH^+ modes are between 3000 and 3225 cm^{-1}. The vibrational mode at lowest frequency is associated with the NH^+ → *C*-terminus hydrogen bond, while the other two correspond to NH^+ → backbone carbonyl interactions. Note that, in a few cases, for example, the lowest-frequency NH^+ vibration in A_73, the DFT normal modes predict coupling between the NH and CH stretches, leading to the predicted doublet at 3015 cm^{-1}. This is likely due to slight inaccuracies in the normal mode coordinates, but in any case is not verifiable in this work.

As with the shorter peptides, the experimental IR band at ~3575 cm^{-1} most likely corresponds to a free OH stretch, identifying A_73 as a strongly populated conformer. Indeed, the spectrum predicted for A_73 alone could explain most of the major spectral features, notably (and uniquely) the IR bands between 3100 and 3300 cm^{-1}, but the widespread absorption lying between 3300 and 3500 cm^{-1} suggests an important contribution also from the conformer A_72 and perhaps A_71, although its contribution is unlikely based on the MP2 energies listed in Table 1. In any case, A_73, where the protonated *N*-terminus is fully charge-solvated, can be identified as a major component of Ala_7H^+: all three NH^+ groups are involved in hydrogen bonding to create a globular peptide conformation.

4. Discussion

Combination of the photochemical protonation scheme, 1−4, with R-IRMPD spectroscopy in the OH and NH stretch regions as well as DFT and MP2 calculations has allowed an investigation of the conformational landscapes of a series of protonated alanine polypeptides isolated in the gas phase at temperatures of ~350 K and, most importantly, of their structural evolution with increasing chain length. The complementary theoretical investigations have led to the identification of some hydrogen bonding motifs in the protonated peptides and the structural information associated with local minima on their conformational landscapes.

The peptide vibrational spectral signatures, presented in Figures 2B, 3B, 4B, and 6B have allowed different peptide conformations to be distinguished through analysis of their R-IRMPD bands in the NH and OH stretch regions. In general, free backbone NH stretch modes are predicted to appear around

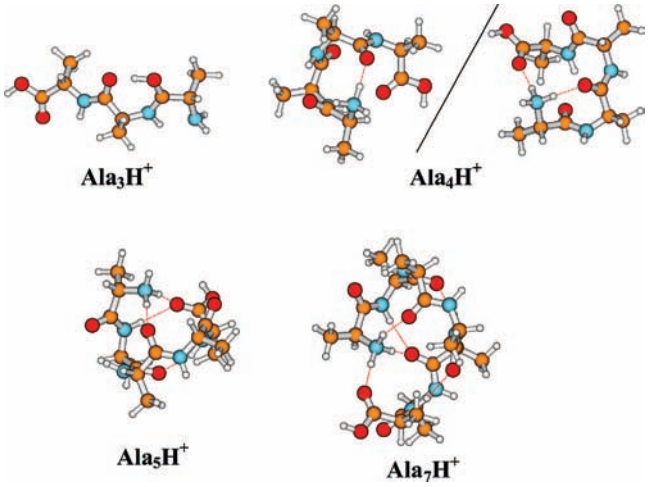

Figure 7. Summary of the dominant Ala_nH^+ conformers identified in this work. Note also that the present results and analyses cannot unambiguously differentiate between A_42 and A_43 (both may be present in nearly equal populations).

~3400 cm^{-1}; weakly hydrogen-bonded backbone NH modes (*e.g.*, NH−carbonyl interactions), as well as free NH^+ modes, are broadly located around ~3300 cm^{-1}; and strongly hydrogen-bonded NH^+ modes, such as the charge-solvating NH^+-*C*-terminal hydrogen-bonded mode, appear at low wavenumbers, anywhere from ~3200 to ~2600 cm^{-1}. These predictions have been validated by the experimental observations, although the correlation of the predicted NH (and OH) vibrational transitions for DFT structures to the R-IRMPD spectra requires some caution. The relationship between the natural intensity of an IR absorption band and its R-IRMPD intensity is unclear, especially in the less-characterized OH/NH stretch region, and the scaled wavenumbers for the hydrogen-bonded NH^+ modes (the most "diagnostic" modes), computed through DFT calculations may not be accurate. Furthermore, the protonated peptide cations have relatively high internal energy contents, and thus, their zero-temperature structures and vibrational modes may not provide completely accurate descriptions given the possibility that barriers between some conformers may be fairly low. Indeed, a more rigorous approach would be to use the CPMD simulation method of Gaigeot and co-workers.[22] Despite these caveats, however, the results have been very encouraging: the broad, general agreement between predicted and observed spectral features has allowed some conformational assignments to be made and, perhaps more importantly, has revealed the evolution of the preferred protonated peptide structures with increasing chain length, from extended, to cyclic, to globular. The results support the seminal ion mobility and molecular dynamics studies by Jarrold and co-workers that first revealed globular, charge-solvated Ala_nH^+ conformations (through mass spectrometric rather than optical spectroscopic detection).

To highlight the structural evolution, the dominant conformations identified in each of the Ala_nH^+ (n = 3, 4, 5, and 7) peptides, based on the analyses presented above, are summarized in Figure 7. The *O*-protonated Ala_3H^+ conformer shown (A_31) is representative of an unfolded peptide; a small population of (*N*-protonated) cyclic hydrogen-bonded conformers is also present, but intramolecular H-bonding does not likely confer conformational stability. In contrast, addition of the fourth amino acid residue allows the Ala_4H^+ peptide to fold, although unambiguous differentiation of the A_42 and A_43 conformers is not possible here. Both the spectroscopic observation of intense hydrogen-bonded NH^+ stretch bands and the DFT and MP2 calculations indicate the onset of cyclic structures, promoted through *N*-terminus → *C*-terminus hydrogen bonding. Additional extension of the peptide chain allows the Ala_5H^+ peptide to adopt a globular (and perhaps also cyclic) conformation, although there is very little intramolecular hydrogen bonding not involving the *N*- and *C*-termini. Finally, when the chain is extended still further, to Ala_7H^+, the peptide shape becomes purely globular. This change is signaled by the distinctive appearance of its vibrational signature (see Figure 1) which presents a new, broad feature centered around 3175 cm^{-1}, associated with NH^+ → carbonyl backbone interactions. All three *N*-terminal NH^+ groups are involved in hydrogen bonding, and the charged *N*-terminus is "buried" in the globular peptide. The globular structure is also supported by NH → carbonyl hydrogen bonds *not* involving the *N*- or *C*-termini. Such interactions are important for "real-world" folding into physiological secondary structure. Ala_7H^+ is globular as predicted, but its peptide backbone is now long enough to allow other folding interactions.

A final word pertains to the warm nature of the protonated peptides investigated in the current work. First, it appears that the initial prediction of internal energies corresponding roughly to room-temperature (or slightly higher temperature) conditions is validated by the observation of hydrogen-bonded conformations, which would likely be disrupted at much higher internal energies as well as the relatively narrow R-IRMPD bands, especially for the longer peptides. Next, while the experimental conditions do not allow characterization of their global minimum-energy conformations at low temperature, they do allow identification of their free energetically favored conformations. The relative energies and free energies in Table 1 demonstrate the important role that entropy can play in governing their conformational landscapes. In Ala_3H^+, the entropically favored *O*-protonated species is dominant, whereas the enthalpically favored *N*-protonated conformer is only minimally present. In Ala_4H^+, Ala_5H^+, and Ala_7H^+, the OH group in the lowest-energy conformer at 0 K is hydrogen-bonded to a neighboring backbone carbonyl group. However, their experimental R-IRMPD spectra show that the OH group is free in their most populated conformations. This is reflected in their relative MP2 free energies, calculated at 350 K: conformers with a free OH become more favorable at 350 K.

5. Conclusions

R-IRMPD spectroscopy of OH and NH (and CH) stretch modes, along with complementary DFT calculations, provides a powerful means of investigating the conformational landscapes of short to moderate-length protonated peptides, free of environmental effects in the gas phase. The internal energy content in the photochemically generated, longer-chain protonated peptides is low enough to sustain population of their hydrogen-bonded conformations, clearly signaled by the appearance of intense NH stretch bands shifted to low wavenumbers. When their observed vibrational spectra are matched to those predicted through DFT calculation, they reveal the three-dimensional shapes of the peptides, their conformational evolution with increasing chain length, and the roles of protonation and intramolecular hydrogen bonding on their conformational landscapes.

The peptide Ala_3H^+ exhibits an unfolded shape with likely dynamic interconversion between different conformations. The results are consistent with predominantly *O*-protonated peptides with small contributions from hydrogen-bonded *N*-protonated species. The Ala_4H^+ peptide can adopt both cyclic and globular

charge-solvated shapes protonated at the *N*-terminus. In the longest peptide Ala_7H^+, the protonated *N*-terminus can become fully charge-solvated and the long peptide backbone allows "physiologically relevant" intramolecular NH → carbonyl hydrogen bonding. These results are all consistent with conclusions drawn from previous mass spectrometric, molecular dynamics, and FEL-spectroscopic investigations.

The successful application of R-IRMPD spectroscopy conducted in the OH and NH stretch region to the study of protonated gas-phase peptide structure and conformation is very encouraging. Even though the specific peptide conformational structures are not always identifiable, spectroscopic and general conformational "patterns" may be recognizable and can yield valuable information. The way is now clear for its extension to explore and understand the effects of protonation on the noncovalent intra- (and inter-) molecular interactions in larger and more complex biologically relevant systems and how they govern the conformational landscapes and eventually, physiological behavior, of biological molecules.

Acknowledgment. The authors are grateful for the support provided by the Royal Society USA/Canada Research Fellowship (TDV) and University Research Fellowship (LCS); the Leverhulme Trust (Grant F/08788G); Deutsche Forschungsgemeinschaft (Grant SU 244/3-1, SS and BP); Corpus Christi College, Oxford (TSJAB and LCS), Linacre College, Oxford (TDV) and the Physical and Theoretical Chemistry Laboratory. The authors are also grateful for experimental assistance provided by Dr. Jann Frey.

Supporting Information Available: Additional data. This material is available free of charge via the Internet at http://pubs.acs.org.

References and Notes

(1) Brenner, V.; Piuzzi, F.; Dimicoli, I.; Tardivel, B.; Mons, M. *J. Phys. Chem. A* **2007**, *111*, 7347.
(2) Chin, W.; Piuzzi, F.; Dimicoli, I.; Mons, M. *Phys. Chem. Chem. Phys.* **2006**, *8*, 1033.
(3) Snoek, L. C.; Robertson, E. G.; Kroemer, R. T.; Simons, J. P. *Chem. Phys. Lett.* **2000**, *321*, 49.
(4) Haber, T.; Seefeld, K.; Kleinermanns, K. *J. Phys. Chem. A* **2007**, *111*, 3038.
(5) Abo-Riziq, A.; Crews, B. O.; Callahan, M. P.; Grace, L.; de Vries, M. S. *Angew. Chem., Int. Ed.* **2006**, *45*, 5166.
(6) De Vries, M. S.; Hobza, P. *Annu. Rev. Phys. Chem.* **2007**, *58*, 585.
(7) Compagnon, I.; Oomens, J.; Meijer, G.; Von Helden, G. *J. Am. Chem. Soc.* **2006**, *128*, 3592.
(8) Paizs, B.; Suhai, S. *Mass Spectrom. Rev.* **2005**, *24*, 508.
(9) Zhang, Z.; Bordas-Nagy, J. *J. Am. Soc. Mass Spectrom.* **2006**, *17*, 786.
(10) Lifshitz, C. *Int. J. Mass Spectrom.* **2004**, *234*, 63.
(11) Wyttenbach, T.; Paizs, B.; Barran, P.; Breci, L.; Liu, D.; Suhai, S.; Wysocki, V. H.; Bowers, M. T. *J. Am. Chem. Soc.* **2003**, *125*, 13768.
(12) Jarrold, M. F. *Annu. Rev. Phys. Chem.* **2000**, *51*, 179.
(13) Jarrold, M. F. *Phys. Chem. Chem. Phys.* **2007**, *9*, 1659.
(14) Barran, P. E.; Polfer, N. C.; Campopiano, D. J.; Clarke, D. J.; Langridge-Smith, P. R. R.; Langley, R. J.; Govan, J. R. W.; Maxwell, A.; Dorin, J. R.; Millar, R. P.; Bowers, M. T. *Int. J. Mass Spectrom.* **2005**, *240*, 273.
(15) McColl, I. W.; Blanch, E. W.; Hecht, L.; Kallenbach, N. R.; Barron, L. D. *J. Am. Chem. Soc.* **2004**, *126*, 5076.
(16) Shi, Z.; Olson, C. A.; Rose, G. D.; Baldwin, R. W.; Kallenbach, N. R. *Proc. Natl. Acad. Sci. U.S.A.* **2002**, *99*, 9190.
(17) Wei, Y.; Nadler, W.; Hansmann, U. H. E. *J. Chem. Phys.* **2007**, *126*, 204307.
(18) Hudgins, R. R.; Mao, Y.; Ratner, M. A.; Jarrold, M. F. *Biophys. J.* **1999**, *76*, 1591.
(19) Stearns, J. A.; Boyarkin, O. V.; Rizzo, T. R. *J. Am. Chem. Soc.* **2007**, *129*, 13820.
(20) Polfer, N. C.; Oomens, J.; Suhai, S.; Paizs, B. *J. Am. Chem. Soc.* **2007**, *129*, 5887.
(21) Gregoire, G.; Gaigeot, M. P.; Marinica, D. C.; Lemaire, J.; Schermann, J. P.; Desfrancois, C. *Phys. Chem. Chem. Phys.* **2007**, *9*, 3082.
(22) Marinica, D. C.; Gregoire, G.; Desfrancois, C.; Schermann, J. P.; Borgis, D.; Gaigeot, M. P. *J. Phys. Chem. A* **2006**, *110*, 8802.
(23) Stearns, J. A.; Guidi, M.; Boyarkin, O. V.; Rizzo, T. R. *J. Chem. Phys.* **2007**, *127*, 154322.
(24) Stearns, J. A.; Mercier, S.; Seaiby, C.; Guidi, M.; Boyarkin, O. V.; Rizzo, T. R. *J. Am. Chem. Soc.* **2007**, *129*, 11814.
(25) Vaden, T. D.; De Boer, T. S. J. A.; MacLeod, N. A.; Marzluff, E. M.; Simons, J. P.; Snoek, L. C. *Phys. Chem. Chem. Phys.* **2007**, *9*, 2549.
(26) MacLeod, N. A.; Simons, J. P. *Mol. Phys.* **2007**, *105*, 689.
(27) Vaden, T. D.; de Boer, T. S. J. A.; Simons, J. P.; Snoek, L. C. *Phys. Chem. Chem. Phys.* **2008**, *10*, 1443.
(28) Oomens, J.; Satarkov, B. G.; Meijer, G.; von Helden, G. *Int. J. Mass Spectrom.* **2006**, *254*, 1.
(29) Liu, D.; Wyttenbach, T.; Barran, P. E.; Bowers, M. T. *J. Am. Chem. Soc.* **2003**, *125*, 8458.
(30) Paizs, B.; Suhai, S. *J. Am. Soc. Mass Spectrom.* **2004**, *15*, 103.
(31) Case, D. A.; Pearlman, D. A.; Caldwell, J. W.; Cheatham, T. E., III; Ross, W. S.; Simmerling, C. L.; Darden, T. A.; Merz, K., M.; Stanton, R. V.; Cheng, A. L.; Vincent, J. J.; Crowley, M.; Tsui, V.; Radmer, R.; Duan, Y.; Pitera, J.; Massova, I. G.; Seibel, G. L.; Singh, U. C.; Weiner, P. J.; Kollmann, P. A. University of California: San Francisco.
(32) Frisch, M. J.; Trucks, G. W.; Schlegel, H. B.; Scuseria, G. E.; Robb, M. A.; Cheeseman, J. R.; Montgomery, J., J. A.; Vreven, T.; Kudin, K. N.; Burant, J. C.; Millam, J. M.; Iyengar, S. S.; Tomasi, J.; Barone, V.; Mennucci, B.; Cossi, M.; Scalmani, G.; Rega, N.; Petersson, G. A.; Nakatsuji, H.; Hada, M.; Ehara, M.; Toyota, K.; Fukuda, R.; Hasegawa, J.; Ishida, M.; Nakajima, T.; Honda, Y.; Kitao, O.; Nakai, H.; Klene, M.; Li, X.; Knox, J. E.; Hratchian, H. P.; Cross, J. B.; Adamo, C.; Jaramillo, J.; Gomperts, R.; Stratmann, R. E.; Yazyev, O.; Austin, A. J.; Cammi, R.; Pomelli, C.; Ochterski, J. W.; Ayala, P. Y.; Morokuma, K.; Voth, G. A.; Salvador, P.; Dannenberg, J. J.; Zakrzewski, V. G.; Dapprich, S.; Daniels, A. D.; Strain, M. C.; Farkas, O.; Malick, D. K.; Rabuck, A. D.; Raghavachari, K.; Foresman, J. B.; Ortiz, J. V.; Cui, Q.; Baboul, A. G.; Clifford, S.; Cioslowski, J.; Stefanov, B. B.; Liu, G.; Liashenko, A.; Piskorz, P.; Komaromi, I.; Martin, R. L.; Fox, D. J.; Keith, T.; Al-Laham, M. A.; Peng, C. Y.; Nanayakkara, A.; Challacombe, M.; Gill, P. M. W.; Johnson, B.; Chen, W.; Wong, M. W.; Gonzalez, C.; Pople, J. A. *Gaussian 03, Revision C.02*; Gaussian, Inc: Pittsburgh, PA, 2003.
(33) Andrei, H.-S.; Solca, N.; Dopfer, O. *ChemPhysChem* **2006**, *7*, 107.
(34) Zwier, T. S. *J. Phys. Chem. A* **2001**, *105*, 8827.
(35) Wu, R.; McMahon, T. B. *J. Am. Chem. Soc.* **2007**, *129*, 11312.
(36) Hammer, N. I.; Diken, E. G.; Roscioli, J. R.; Johnson, M. A.; Myshakin, E. M.; Jordan, K. D.; McCoy, A. B.; Huang, X.; Bowman, J. M.; Carter, S. *J. Chem. Phys.* **2005**, *122*, 244301.
(37) Roscioli, J. R.; McCunn, L. R.; Johnson, M. A. *Science* **2007**, *316*, 249.

JP800069N